The Orbital Motion and Impact Circumstances of Comet Shoemaker-Levy 9

Paul W. Chodas
301-150G
Jet Propulsion Laboratory
Pasadena, CA 91109
Phone: (818) 354-7795
FAX: (818) 393-1159
E-mail: paul.w.chodas@jpl.nasa.gov

Donald K. Yeomans
301-150G
Jet Propulsion Laboratory
Pasadena, CA 91109
Phone: (818) 354-2627
FAX: (818) 393-1159
E-mail: donald.k.yeomans@jpl.nasa.gov

To be Published in *The Collision of Comet Shoemaker-Levy 9 and Jupiter*
Edited by K.S. Noll, P.D. Feldman, and H.A. Weaver
Cambridge University Press, 1996

The orbital motion and impact circumstances of Comet Shoemaker-Levy 9

By PAUL W. CHODAS and DONALD K. YEOMANS

Jet Propulsion Laboratory, California Institute of Technology, 4800 Oak Grove Drive, Pasadena, CA 91109, USA

Two months after the discovery of comet Shoemaker-Levy 9 came the astonishing announcement that the comet would impact Jupiter in July 1994. Computing the orbital motion of this remarkable comet presented several unusual challenges. We review the pre-impact orbit computations and impact predictions for SL9, from the preliminary orbit solutions shortly after discovery to the final set of predictions before the impacts. The final set of predicted impact times were systematically early by an average of 7 minutes, probably due to systematic errors in the reference star catalogs used in the reduction of the fragments' astrometric positions. The actual impact times were inferred from the times of observed phenomena for 16 of the impacts. Orbit solutions for the fragments were refined by using the actual impact times as additional data, and by estimating and removing time-varying biases from the astrometric observations. The final orbit solutions for 21 fragments are tabulated, along with final estimates of the impact times and locations. The pre-breakup orbital history of the comet was investigated statistically, via a Monte Carlo analysis. The progenitor nucleus of SL9 was most likely captured by Jupiter around 1929 ± 9 years. Prior to capture, the comet was in a low-eccentricity, low-inclination heliocentric orbit entirely inside Jupiter's orbit or (less likely) entirely outside. The ensemble of possible pre-capture orbits is consistent with a group of Jupiter family comets known as the quasi-Hildas.

1. Introduction

The late-March 1993 discovery of multiple comet Shoemaker-Levy 9 by Carolyn and Gene Shoemaker and David Levy set in motion an extraordinary international effort to study the evolution of a remarkable cometary phenomenon and to witness its ultimate collision with Jupiter (Shoemaker *et al.* 1993). From the beginning, it was clear that the orbital dynamics of this comet were unique. It had spectacularly split into ~ 20 fragments, most likely because of tidal disruption during a recent very close approach to Jupiter. Preliminary orbit computations soon confirmed the close approach, and revealed the surprising fact that the comet was actually in orbit about the planet (Marsden 1993b). Even more extraordinary news came several weeks later, when further orbit computations suggested that the comet would likely collide with Jupiter in late July 1994 (Nakano 1993, Yeomans and Chodas 1993a). Early calculations indicated that the collision would take place on the far side of the planet as viewed from the Earth, but the precise location was very uncertain. After the comet emerged from solar conjunction in December 1993, important new astrometric measurements were added to the data set, and the predicted impact locations moved much closer to the limb of Jupiter, although they were still on the far side (Yeomans and Chodas 1993b). During the months leading up to the impacts, increasingly more accurate predictions of the impact times and locations were computed and distributed electronically to the astronomical community. These predictions made it possible for the extraordinary impact events to be well recorded by an unprecedented array of ground-based and space-based instruments.

Orbital computations for comet Shoemaker-Levy 9 (referred to as SL9 hereafter) presented several challenges beyond what is normally the case for comets and asteroids.

Because the comet was in orbit about Jupiter and was heading for an impact, new parameters such as jovicentric positions and velocities in various reference frames, jovicentric orbital elements, impact times, and impact locations had to be computed. Since the comet had fragmented into a string of nuclei with no obvious bright central condensation to use as a reference point, astrometric measurements and orbit computations were referenced to the mid-point of the string, which was rather ill-defined. Eventually, the mid-point was abandoned in favor of tracking to approximately 20 individual fragments, requiring that orbit computations and impact predictions be repeated for each nucleus. Determining the orbits for some of the smaller fragments was difficult, since very little astrometric data were available for these poorly observed objects. Some of the fragments disappeared completely as the comet evolved, while others split. Proper identification of fragments was a problem, as they were sometimes mislabeled in the astrometric data. Detective work was required to sort out fragment identities. Even Mother Nature conspired to add confusion, when a telescope observing SL9 from Kitt Peak in Arizona was unknowingly shaken during the January 17, 1994 earthquake in southern California. The effect of the earthquake on these astrometric observations was detected only through the resulting large orbit residuals.

Accurately determining the motion of the fragments close to the July 1994 impacts offered additional computational challenges. The need for accurate impact predictions required the modeling of the perturbing effects of the Galilean satellites and Jupiter's oblateness. Also, as the fragments approached the planet, their motion became very non-linear. The fact that our software used a variable integration step size, and that the partial derivatives required in the orbital differential correction process were numerically integrated along with the comet's motion rather than being approximated using finite differences, allowed us to refine the orbit solutions right up to the times of impact.

In the next section, we review the pre-impact orbit computations and impact predictions for SL9, from the preliminary orbit solutions shortly after discovery to the final set of predictions before the impacts. We then discuss post-impact analyses, indicating how the observed impact phenomena were interpreted, and how the actual impact times were inferred. We give a compilation of the times of key events in the observed light curves. Following this, we describe how the orbit solutions were improved after the impacts, by using the actual impact times as additional data and by removing measurement biases from the astrometric observations. We tabulate our final orbit solutions for 21 fragments, in both heliocentric and jovicentric form. Next, we present our final estimates of the impact times, locations, and geometries as derived from the final orbit solutions. Finally, we discuss the pre-breakup orbital history of the comet, which we have investigated statistically using a Monte Carlo analysis. We give our estimate of when the comet was likely captured by Jupiter, and characterize SL9's possible pre-capture heliocentric orbits.

2. Pre-impact orbital analyses and impact predictions

The early orbital analyses of SL9 were based on the supposition that the comet had broken up during a recent close approach to Jupiter. The circumstantial evidence was strong: SL9 had split into a large number of fragments in a well organized geometry, and it was currently situated only 4 degrees from the largest planet in the Solar System. Tidal disruption during an approach to within the Roche limit of a large perturbing body is a common mechanism for cometary splitting. Several comets have been known to split after close approaches to the Sun and Jupiter, P/Brooks 2, is known to have split after approaching Jupiter to ~ 2 Jupiter radii (R_J) in July 1886 (Sekanina and Yeomans

1985). Thus, the supposed breakup scenario would not be unprecedented. It was far from a certainty, however, as comets have been seen to split spontaneously, when nowhere near a large body. The day after the announcement of the comet's discovery, B. G. Marsden published a very preliminary orbit solution in which he used the assumption of a close passage by Jupiter (Marsden 1993a). His computations suggested that the comet's close approach to the planet had been at a distance of 0.04 AU in late July 1992, surprisingly accurate considering how little data were used in the solution. It would be many weeks before enough astrometric data became available to confirm that the comet had indeed made an extremely close approach to Jupiter on July 7, 1992, at a distance of only 1.3 R_J from the center of the planet.

Computing the orbit of SL9 in the first month or so after its discovery was very difficult. Few astrometric measurements were available, and the presence of nearby Jupiter introduced a large nonlinearity into the orbit computations. Furthermore, SL9 had no single central condensation to serve as a reference point for astrometric measurements. Since the individual nuclei were not easily resolvable by many observers, the convention was adopted to measure only the center of the train of nuclei, the mid point of the bar (Marsden 1993b). This simplifying assumption greatly facilitated astrometry for many observers, especially amateurs, who provided a large fraction of the early measurements. We certainly would not have learned as much as we did about the orbit of SL9 as quickly as we did without this convention. However, the center of the train was rather ill-defined, and different observers placed it at different points in the train, according to the extent of the train each could see. Moreover, as the length of the train grew, errors in locating its center also grew.

A week after his first orbit solution, Marsden (1993b) obtained an improved solution which indicated a surprising new result: SL9 appeared to be in orbit about Jupiter. This was also not unprecedented. Carusi *et al.* (1985) investigated the long-term motion of all periodic comets with well known orbits and found several that had either been in temporary Jupiter orbit in the past, or would enter temporary orbit in the relatively near future. Tancredi *et al.* (1990) investigated the temporary capture of comet P/Helin-Roman-Crockett by Jupiter during intervals centered on close approaches to Jupiter in 1976 and 2075. Using more recent orbit solutions, with nongravitational effects included when appropriate, we studied the motions of seven comets other than SL9 that either have been, or will be, temporary satellites of Jupiter (Yeomans and Chodas 1994b).

By early May, the span of astrometric observations was sufficiently long to begin to reveal the true collision trajectory of the comet. Amateur observers had contributed a large number of valuable measurements, and as more and more of these were used, orbital computations by S. Nakano and Marsden began to indicate the possibility of impact in July 1994. Now, this was truly unprecedented. Marsden alerted us of this exciting development on May 21, and provided the latest of recent astrometric measurements. We immediately confirmed Nakano and Marsden's computations, and computed that the probability of impact was about 50%. Our software had just recently been augmented with the capability to estimate probabilities of impact, in preparation for a study of the hazards of near-Earth objects (Chodas 1993, Yeomans and Chodas 1995). The dramatic announcement of the impending collision was issued the next day (Marsden 1993c), along with Nakano's orbit solution (Nakano 1993). One of our initial orbit solutions appeared in the Minor Planet Circulars shortly after (Yeomans and Chodas 1993b). Within a few days of the impact announcement, as more astrometric data became available, the probability of impact rose to 64% (Yeomans and Chodas 1993a), and it reached 95% only a week later.

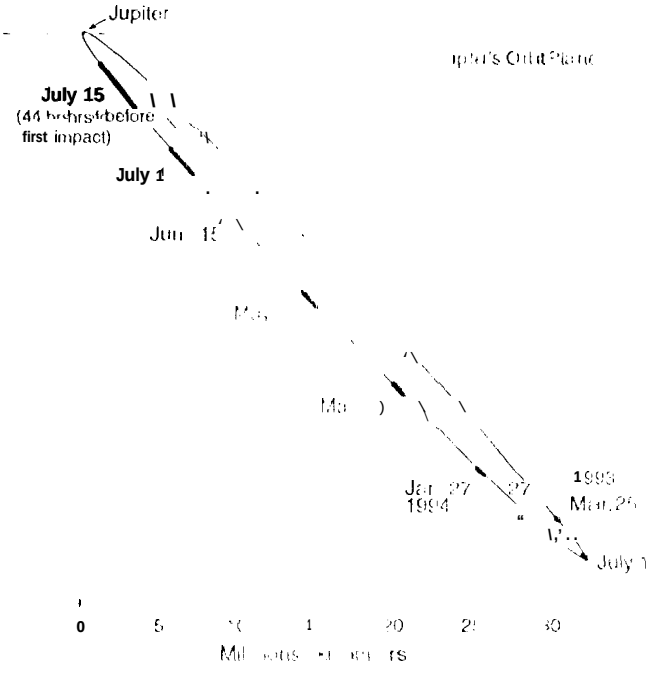

Figure 1. The orbit of comet Shoemaker-Levy 9 about Jupiter, as viewed from the direction of Earth on May 15, 1994. The length and orientation of the train of fragments are shown to scale on eight dates. The train is nearly aligned along the velocity vector, except near apojove. The orbit is somewhat foreshortened in this view; the major axis rises out of the plane of the diagram towards the viewer at an angle of about 20 degrees.

To determine the basic characteristics of SL9's orbit and its impending impact, we quickly modified our software to provide geocentric information, including position, velocity, and orbital elements as a function of time. It became clear that the comet was approaching the apojove of an extremely eccentric orbit about Jupiter, with eccentricity ~ 0.99 and apojove distance ~ 0.33 AU (see Fig. 1). By June 1, we had determined that the impact would occur in the mid southern latitudes of Jupiter, and, unfortunately, on the side of the planet facing away from Earth. We defined impact to occur when the comet reached the one bar pressure level in Jupiter's atmosphere, which we modeled as an oblate spheroid with radius and flattening given by Davies *et al.* (1992). Finding the moment of impact in these early solutions required searching through tables of numbers, but we soon automated this important function. We also wrote software to compute and plot the motion of the comet in various jovicentric frames, which helped in visualizing its trajectory (Yeomans and Chodas 1993). With it, we determined that the Galileo spacecraft would likely have a direct view of the impact, although this was far from certain because the predicted impact was right on the limb.

There was much more to study with this dynamically fascinating object. For one thing, it had a whole train of nuclei to consider. As SL9 passed through apojove around July 13, the question arose as to whether the fragments would reverse their order on the sky as viewed from the Earth. After all, they had 'turned the corner' and were heading back to Jupiter. But in fact, the appearance of the train did not change because the fragments were not all on the same orbit. A useful analogy is to think of throwing a handful of pebbles upwards, each receiving a slightly different vertical velocity. The slowest pebble

trails the others going upwards, but it reaches its apex first and is the first to hit the ground; furthermore, the separations between the pebbles increase monotonically during their flight. With SL9, the easternmost fragment trailed the others on the outbound leg, reached apojove first, and became the leading fragment inbound. The fragments passed through apojoves in sequence over a period of a few days, while the train continued its expansion and remained approximately pointed at Jupiter throughout.

As SL9 headed into solar conjunction in late July, other important questions were being raised. Would all the fragments collide with Jupiter? Would any of them impact on the side of Jupiter visible from Earth? Unfortunately, no astrometric measurements of individual nuclei were available for computing orbit solutions. In anticipation of their availability, however, we wrote new software to investigate how slight variations in an object's orbit at one epoch would affect its position on the plane of sky at later epochs. We would soon use this software to study the tidal splitting of the comet and explain the appearance of the train. Scotti and McNaught (1993) used a similar model when, armed with Scotti's measurements of the train length and orientation, they determined that the progenitor nucleus needed to be only 1 km in radius to explain the observed train dimensions, assuming disruption occurred at perijove. They also determined that the entire train would impact Jupiter over a period of 5.6 days. With Scotti's train measurements in hand, and using their assumptions, we confirmed these results and furthermore determined that all the fragments would impact Jupiter on the far side as viewed from Earth.

The first astrometric measurements of individual nuclei became available in October 1993. These were positions of 21 fragments obtained by Jewitt *et al.* (1993) on four nights from March through July, 1993. The positions were offsets from the brightest nucleus, designated 7 in Jewitt's numbering system. In collaboration with Z. Sekanina, we determined the effective time of tidal disruption and the impulse each fragment must have received in order to appear at the observed relative positions. This approach provided the first orbital solutions and predicted impact times for individual fragments, which we denoted A through W (Chodas and Yeomans 1993). Because the relative times were known much better than the absolute times, these first impact time predictions were given relative to the impact time of the center of the train. The relative times all turned out to be within 40 minutes of the actual impact times relative to the center time, remarkable precision considering the prediction for each fragment was based on only 4 measurements taken over a year before impact. This accuracy attests to the precision of Jewitt *et al.*'s measurements, and indicates the great utility of the tidal disruption approach for computing orbit solutions. Our orbit solutions indicated that, to match the observed position angle history of the train to the 0.1 degree level, the effective time of tidal breakup of the progenitor comet had to be ~ 2.2 hr after perijove passage in 1992. From this and other evidence, we concluded that the radius of the progenitor comet was probably ~ 5 km. (Sekanina *et al.* 1994).

Other important predictions required at this time included the expected uncertainties of the predicted impact times in the last weeks and days before impact. The impact time accuracy was required to plan impact observations, especially those to be made by spacecraft, which had to programmed well in advance of the event. The rate of decrease of the impact time uncertainty depended upon the number of the astrometric measurements used in the orbit solutions, as well as their quality. Assuming a conservative 9 measurements per month and a fair set of measurement accuracy, we estimated the 1-sigma impact time uncertainty a month before impact would be ~ 13 minutes, and a week before impact, ~ 7 minutes. If only two more measurements could be made on the two days before impact, the uncertainty would drop to ~ 3 minutes. Clearly, the most

powerful observations for determining impact times were those closest to impact. But how close to bright Jupiter could the faint cometary fragments be observed?

In November, the first batches of absolute astrometric measurements for individual fragments became available: J. V. Scotti and J. Metcalfe provided 250 measurements obtained from Kitt Peak over the period March through July, and A. Whipple and P. Shelus provided 54 measurements obtained from McDonald Observatory taken in April and May. Marsden (1993d) used the Kitt Peak data to compute the first independent orbit solutions for individual fragments (i.e., solutions which made no assumptions about the tidal disruption process), and we used these observation sets in similar solutions a few days later. Only the nine brightest fragments (E, G, H, K, L, Q, R, S, and W) had enough astrometric data to yield well-determined solutions. The impact times derived from these solutions were about 18 hours earlier than those based on the center-of-train solution and relative astrometry. This jump was most likely due to errors in locating the center of the train: the east end of the train may have been too faint to be seen by many of the observers. The new orbit solutions superceded the center-of-train solutions, which were now abandoned; astrometry and orbit computations from this time onwards referred only to individual fragments. The impact time uncertainties actually increased slightly with the new solutions, because the fragments had fewer measurements than the center-of-train orbits, but at least the solutions were now tied to well-defined points.

The emergence of SL9 from solar conjunction was greatly anticipated. Although attention focused on possible changes in the appearance of the comet, we were anxious because new astrometric data would dramatically improve the orbit solutions. On December 9, sooner than expected, Scotti recovered the comet. Although the train had lengthened, the fragments appeared much the same as before conjunction. Marsden (1993e) computed new orbit solutions for the nine brightest fragments and found that the impact times were almost a day earlier than in previous solutions. We confirmed Marsden's computations, and found an exciting new result: the predicted impact locations, though still on the far side of Jupiter, were now much closer to the morning terminator, only 5–10 degrees behind the limb as seen from the Earth, with the later impacts closest to the limb (Yeomans and Chodas 1993c, Chodas and Yeomans 1994a). The impact sites had also moved well onto the hemisphere visible to Galileo. Would the predicted impact locations continue to move towards the limb, and possibly even onto the near side? Unfortunately not. These would be the last large changes in the predictions, because the orbit solutions had become relatively well determined. Based on Monte Carlo analyses which used actual orbit uncertainties and perturbations, we concluded that there was little chance that any of the fragments would impact the side of Jupiter visible to the Earth.

In mid-December, our impact predictions, together with orbital elements and ephemerides for the nine brightest fragments, were posted on the special SL9 electronic bulletin board operated at the Planetary Data Systems Small Bodies Node at the University of Maryland (UMD). Over the remaining seven months before impact, we posted over a dozen more sets of predictions and associated data. The predicted parameters in our tables included impact time, jovicentric latitude, meridian angle, and the Earth-Jupiter-fragment (E-J-F) angle at impact. This latter angle indicated how far behind the limb the impact would occur. The meridian angle was defined as the jovicentric longitude of impact relative to the midnight meridian, measured towards the morning terminator. This relative longitude was known much more accurately than the Jupiter-fixed longitude, because of the large uncertainty in the impact times and Jupiter's fast rotation. Basically, the approach trajectory of each fragment was known much more accurately than the fragment's location on that trajectory at any given time. Predictions of absolute jovicentric longitude were not included in our tables until later, when the

impact times were better known. Also archived later were predictions of satellite longitudes at impact for four of the inner jovian satellites: Amalthea, Io, Europa, and Ganymede, kindly supplied by P. D. Nicholson.

Keeping track of all the fragments was a continual challenge. Not only were there a lot of them to consider, but each seemed to have its own personality. In January 1994, only seven fragments (G, H, K, L, Q, S, and W) had well-established orbit solutions and consistent impact predictions, while solutions for E and R remained a little erratic, as they were based on fewer measurements. The rest of the fragments had too little astrometric data to determine reliable independent orbit solutions, so we applied our tidal disruption model as we had done earlier, although now we varied the orbit of fragment Q instead of the orbit for the center of the train. By the end of the month, as more observations became available, the solutions for fragments E and R became consistent with the rest, and fragment F graduated to the group with independent solutions. The image of SL9 taken by the Hubble Space Telescope (HST) in late January revealed changes in the SL9 menagerie: fragments J and M had disappeared completely, and fragments in the P-Q region had clearly split. For a time there was confusion in identifying fragments in this region, with N identified as P and the P sub-fragments identified as Q3 and Q4, but by mid-February the P1/P2 and Q1/Q2 nomenclature was established (Marsden 1994a). Correctly identifying the fainter fragments in ground-based observations was a recurring problem, as the fragments were often near the limits of detectability. We checked observer's identifications by comparing observations against positions predicted from orbit solutions, but this was an imperfect process because the orbit solutions for these faint fragments were not well-determined either.

By late February, independent orbit solutions had been computed for 19 fragments by both Marsden (1994b) and ourselves, although only 12 fragments (the original nine, plus F, N, and P2) had solutions reliable enough to be used in our impact predictions (Chodas *et al.* 1994). By early June we had adopted independent orbit solutions for all fragments but Q2, although the impact predictions for the extremely faint fragments T and U continued to be erratic for several more weeks. Fragment Q2 was especially difficult, as it had very few measurements. Using HST measurements of the offset of Q2 from Q1, Sekanina (1995) applied our disruption model to determine that Q2 likely broke away from Q1 in the March-April 1993 period, right around the time of discovery of SL9. Not until July did the separation between Q1 and Q2 increase to the point that many ground-based observers could resolve the two fragments; we finally adopted an independent solution for Q2 in the last set of predictions before its impact.

In April, we upgraded the dynamical models used in our orbit determinations and impact predictions. Up until this time, we had used only point mass perturbations by the sun and planets, with planetary positions and masses taken from JPL planetary ephemeris DE200 (Standish 1990). But now we switched to the more accurate planetary ephemeris DE245, and refined our models to include perturbations due to the Galilean satellites and the J2 and J4 zonal harmonic terms of Jupiter's gravity field. The positions of the Galilean satellites were computed using the analytic theory by Lieske (1977, 1994), while the parameters for Jupiter's gravity field were obtained from Campbell and Synnott (1985). Since the SL9 fragments approached Jupiter from the south, and impacted in the southern hemisphere, they did not come near the Galilean satellites on their final approach, and, as a result, the inclusion of the satellite perturbations had only a minor effect on the impact times. Similarly, the inclusion of the Jupiter oblateness perturbations made only a small difference in the predicted impact times. Both perturbations, however, were important in the long term backward integration of the comet's motion, discussed in section 6.

As SL9 passed through opposition in the April-May 1994 period, the number of astrometric observations increased dramatically, and the measurements themselves became more powerful in reducing orbital uncertainties simply because the Earth was closer to the comet. During this time, the predicted times drifted towards later impact times for most fragments, until, at the end of May, they were about an hour later than they had been in March. Meanwhile, the formal impact time uncertainties fell from about 30 minutes to 18 minutes (1-sigma), for the brightest fragments. The drift in impact times reversed itself in June and early July, with times sliding earlier by 30–50 minutes on average, while the impact time uncertainties fell to less than 10 minutes. The relatively large shifts in predicted impact times were a concern in the period from mid-June to early July, as final predictions had to be made for use in the Galileo impact observation sequences. The spacecraft was programmed to observe during a window of only 20–60 minutes around each of the predicted times. As it turned out, of the 16 impacts observed by Galileo instruments, only one was missed because the event shifted out of the observing window.

The most likely explanation for the large shifts in the predicted impact times was the presence of systematic errors in the reference star catalogs used by observers in reducing their measurements. Star catalog errors can be a major error source for precision orbit determination of comets and asteroids. Since background stars in an astrometric image are used as reference points in determining the position of an object of interest, systematic errors in the tabulated coordinates and proper motions of the reference stars lead to systematic errors in the deduced positions for the object. Most of the astrometric data for SL9 were reduced with respect to versions 1.0 or 1.2 of the *Hubble Space Telescope Guide Star Catalog* (GSC), which contains systematic errors of ~ 0.5 arcsec for some regions of the sky. These errors are significantly larger than the typical errors incurred in actually measuring the position of the nucleus in the image, which could be as small as ~ 0.2 arcsec in the best ground-based observations. In our orbit solutions, we modeled measurement errors simply as zero mean Gaussian noise, and used a standard deviation, or noise value, of 1 arcsec for most observations to account for the star catalog errors.

Since the most powerful astrometric data for reducing uncertainties in the predicted impact times would be those data taken closest to impact, it was especially important to try to reduce systematic star catalog errors in the region occupied by the comet near impact. To this end, J. V. Scotti generated and distributed a special reference star catalog for the region traversed by the comet in the last week before impact. Scotti made offset corrections to GSC reference stars by differencing the positions of stars common to the GSC and the more accurate PPM catalog (Roeser and Bastian 1989). Observations reduced with respect to Scotti's special catalog were assigned a noise value of 0.6 arcsec in our solutions.

A pre-publication version of the Hipparcos star catalog, kindly provided by M. Perryman and C. Turon of the Hipparcos project, was used by R. West and O. Hainaut in the reduction of a number of observations from the European Southern Observatory (ESO) taken between May 1 and July 14, 1994. Because the Hipparcos catalog is known to be highly accurate, systematic star catalog errors should be largely absent from these measurements, and we therefore assigned them noise values of 0.3 arcsec in our solutions. The post-fit root-mean-square (rms) of the ESO observation residuals was about one third the size of the rms of all the residuals.

The ESO group was able to obtain astrometric images close to Jupiter, with enough sensitivity to see even the fainter fragments. These were the last astrometric observations taken of eight of the faintest fragments, ranging from 2.3 to 7 days before impact. Several other groups attempted to observe the SL9 fragments even closer to impact by using coronographs to block out the light from Jupiter, but this proved to be a very difficult

task. Only two groups succeeded in obtaining astrometric data using this approach: D. Rabinowitz and H. Butner at Las Campanas obtained the last astrometric observations of fragments E, G, and L, with E seen only 1.15 days before its impact, and D. Jewitt and D. Tholen on Mauna Kea obtained the last astrometry for fragments P2, Q2, Q1, R, and S, with P2 caught only 1.33 days before its impact. Observations of several fragments even closer to impact were made by the Hubble Space Telescope, but these did not provide astrometry, except for a measurement of Q2 relative to Q1 within 10 hours of the Q2 impact.

Our final set of predicted impact parameters was issued on the UMD e-mail exploder only 4 hours before impact A. The impact time uncertainties were down in the 3–5 minute range (1-sigma) for most of the fragments, not much different from our original projection of 3 minutes made nine months earlier. Although for most of the fragments, observers had not been able to obtain astrometry as close to impact as we had hoped, they had contributed many more measurements than we had anticipated – about 3200 in total, spread over 20 fragments. Extensive and accurate astrometric data had been received from several observatories, including Catalina Station, Kavalur, Klet, Kuma Kogen, La Palma, La Silla, Mauna Kea, McDonald, Siding Spring, Steward, and the U.S. Naval Observatory at Flagstaff. The highly-accurate Hipparcos-based astrometry was also unanticipated, and it contributed greatly to the accuracy of the orbital solutions.

3. Estimates of impact times from observed phenomena

During and after impact week, our attention turned to the problem of determining the actual impact times, based on the timing of observed impact phenomena. This was especially important for maximizing the data return from the Galileo spacecraft, which had viewed the impacts directly. Because of difficulties with its main antenna, the spacecraft had recorded most of its impact observations on tape, and could replay only a small fraction of the data back to Earth. Accurate impact time estimates would help to quickly locate the portions of data obtained around the times of the impacts. Fortunately, observers using Earth-based telescopes and the HST had detected a variety of impact phenomena, and promptly made the times available on the e-mail exploder.

After the first few impact events, it became clear that our predicted impact times were systematically early by 5–10 minutes. This conclusion was based on the assumption that the impacts occurred around the times of the earliest phenomena for each event. Although various types of impact observations were reported, the most robust and consistent set were the phenomena seen in the near-infrared and mid-infrared wavelengths. These light curves followed a consistent pattern, starting with a *precursor* flash, and sometimes even two, followed ~6 minutes later by the start of a dramatic brightening, which later became known as the *main event*. This surprisingly bright feature peaked about 10 minutes after the precursor (see the chapter by Nicholson for details).

The interpretation of the IR light curve features was initially puzzling, with the unusual viewing geometry complicating an already poorly-understood process. The limb of Jupiter just barely occulted the impact sites, and Jupiter's rotation brought them into full view anywhere from 20 minutes later for impact A, to 10 minutes later for W. The precursor was generally believed to be associated with the impact itself, but whether it was the meteor phase being observed directly, or an indirect view of the impact explosion reflected off incoming cometary debris, was not clear. Based on our predictions of how far behind the limb the impacts occurred, the meteors would have to be very high in Jupiter's atmosphere to be visible from Earth, especially for the earlier impacts. The interpretation of the main event was also uncertain. It could not be the plume rising above

the limb of the planet, or the plume creeping into sunlight, because models suggested this would occur only a minute or two after impact (Boslough *et al.* 1994). Another possibility was that the main event was simply the impact site rotating into view, but then there should have been a variation in the time between precursor and main event, according to how far behind the limb the impact occurred.

Confirmation that the IR precursors coincide near the time of impact came from photometric observations obtained by the Photopolarimeter Radiometer (PPR) instrument on board Galileo. Transmitted to Earth within a day of the events, the PPR light curves of the H and L impacts displayed a 2-second rise to peak, followed by a plateau and slow decrease, lasting a total of 25–35 s (Martin *et al.* 1995). The sharp rise was interpreted as corresponding to the final moments of the bolide's trajectory, while the plateau and decay were due to the subsequent expanding and cooling fireball. The times of the initial PPR detection of the H and L impacts matched the times of precursors flashes to within a minute or so, although most of the reported flashes followed the PPR start times by about 1 minute. The PPR times also provided the first accurate calibration of our predicted impact times. The predictions for H and L were an average of 7 minutes early, an effect we subsequently concluded was due to systematic errors in the star catalogs.

Shortly after the impacts ended, we compiled our best estimates of the actual impact times, based on the reported times of various observed phenomena (Yeomans and Chodas 1994a). For impacts H and L, we simply adopted the times of initial detection in the PPR data. For the majority of the other impacts, which had consistent reports of precursor flashes and main events starting 5–6 minutes later, we generally took the impact time to be one minute before the flash time or 6 minutes before the main event start. We also considered a set of impact times determined from measurements of the longitudes of impact spots seen in HST images (Hammel *et al.* 1995). The measured longitudes were differenced with predicted longitudes converted to time differences by dividing by the rotation rate of Jupiter, and added onto the predicted impact times. These times could only be used as guides, however, as they seemed to be uncertain by 3–4 minutes. Finally, for fragments with no observed impact phenomena, we simply added an empirical correction of 7 minutes to the predicted impact times (Chodas and Yeomans 1994b).

The estimates of the actual impact times were used to position the Galileo tape for playback of selected portions of the data during the period from August 1994 through February 1995. Images of impacts K, N, and W taken by the Solid State Imager (SSI) were successfully returned, as were time series of spectra for impacts G and R taken by the Near-Infrared Mapping Spectrometer (NIMS) and Ultraviolet Spectrometer (UVS), as well as a PPR light curve for impact G. To date, Galileo data yielded accurate impact times for a total of 8 impacts: G, H, K, L, N, Q1, R, and W. The new impact time data confirmed our conclusion that the impact predictions were ~ 7 minutes early.

The NIMS light curves for both G and R showed two phases: a fireball phase, due to the hot, expanding plume formed from the impact explosion, and a splash phase attributed to plume material falling back onto the atmosphere, heating it and producing thermal emission. For both the G and R events, the splash phase started ~ 360 seconds after impact, and continued increasing for several minutes, through the end of the data sets (Carlson *et al.* 1995b). The delay between impact and onset of the splash phase seemed to be an intrinsic property of the impactor. Furthermore, it matched the 6 minute delay between first precursor and main event start seen in ground based IR light curves of all the well-observed impacts, suggesting that the onset of the main event was not controlled by observing geometry, and the region of atmospheric heating was directly observable from Earth for most, if not all, the impacts (Zahnle and MacLow 1995).

With this new piece of the puzzle in place, a convincing explanation of the IR light curves was proposed by a number of authors, including Boslough *et al.* (1995), Zahnle and MacLow (1995), Hamilton *et al.* (1995), and Nicholson *et al.* (1995). The scenario, described in detail in the chapters by Nicholson and Sekanina, is summarized as follows. The first precursor (PC1) is due to thermal emission of the meteor trail in the Jupiter's upper atmosphere; its flux peaks as the bolide passes behind the limb, ranging from $\sim$ 15 s before impact for fragment A to $\sim$ 5 s before impact for W. The impact itself occurs at the initial peak of the PPB and SSI light curves, and is not visible from the Earth. At $\sim$ 100 s after impact for A, decreasing to $\sim$ 30 s after impact for W, a self-luminous fireball rises above the limb into Earth view, giving rise to the start of the second precursor (PC2). As the fireball rises and expands, the IR flux increases, but the plume rapidly cools, causing the signal to decay. Still rising, the plume emerges into sunlight, and reaches a maximum height of $\sim$ 3000 km above the 100-mbar pressure level about 8 minutes after impact (Hammel *et al.* 1995). Meanwhile, the main event (ME) starts $\sim$ 360 s after impact, as plume material begins splashing down onto the top of jovian atmosphere.

Table 1 summarizes, in chronological order, the times of key events in the observed impact phenomena, from which we can infer the actual impact times. The list is not meant to be exhaustive: it includes only the Earth-based infrared observations, events observed from Galileo, and relevant images from HST. The data were obtained from published reports, private communications, and a survey of the participants at IAU Colloquium 156. The listed times are generally mid-exposure times, while the uncertainties generally reflect the sampling times of the observations.

We estimated the actual impact times by fitting the times of the observed phenomena to the generic interpretation of light curves described above. These estimates are included in Table 5, along with a host of other results which are discussed later. As an aid in interpreting the impact phenomena, we have included in Table 1 the times of observed events relative to our estimated impact times, T_0. For some of the impact events, the interpretation of phenomena is uncertain, as outlined in the following paragraphs. The orbital solutions referred to in these notes are discussed in the next section.

- Impact A: Hammel *et al.* (1995) suggest that the HST image centered at 20:13:23 UT shows the bolide, since the next frame, centered at 20:15:18 UT shows nothing. Herbst *et al.* (1995) argue that the bright pixels in the first HST frame are due to the plume, since a precursor was seen from Calar Alto over two minutes earlier. Why then does the HST frame at 20:15:18 show nothing? Possibly because it was a short exposure, and possibly because the plume had cooled and had not yet emerged into sunlight. Although Herbst *et al.* could not identify which precursor they saw, due to a data outage, it seems likely that it was PC2. None of the impacts earlier than G produced first precursors, as they were simply too far behind the limb. If the precursor really was PC2, however, it occurs somewhat too soon after our estimated impact time, which was derived from the ME start time. It is possible that the impact occurred $\sim$ 1 minute earlier, and the main event start was delayed because the splash area was entirely beyond the limb. The orbital solutions certainly favor an earlier impact.
- Impact B: The 17-minute duration of the faint event observed from Keck suggests that it was a faint main event, and our impact time estimate is based on this interpretation. However, the orbital solution clearly favors a later impact time, indicating the Keck observation may be a long, second precursor.
- Impact M: We assume the faint bright train seen from Keck was a very faint main event. The orbital solution for this lost fragment is so poorly determined that the predicted impact time cannot assist the interpretation.

Imp	Date	Time (UT)	± (s)	Event	$T - T_*$ (s)	Reference
A	16	20:11:29	5	PC2? start (Calar Alto 2.3 μm)	+ 49	Herbst *et al.* 1995
		20:13:23	7	HST—Bright pixels (888 nm)	+163	Hammel *et al.* 1995
		20:15:18	2	HST—Nothing (888 nm)	+278	Hammel *et al.* 1995
		20:16:56	5	ME start (Calar Alto 2.3 μm)	+376	Herbst *et al.* 1995
		20:18:24	8	HST—Plume in sunlight (953 nm)	+464	Hammel *et al.* 1995
B	17	02:56		ME? start (Keck, 3.3 μm)	+360	de Pater *et al.* 1994
C	17	07:11:57	15	PC2 start (AAT)	+ 67	Meadows, priv. comm.
		07:12:09	30	PC2 start (ANU)	+ 79	McGregor, priv. comm.
		07:12:27	5	PC2 start (Okayama, 2.2 μm)	+ 77	Takeuchi *et al.* 1995
		07:12:42	15	PC2 peak (AAT)	+112	Meadows priv. comm.
		07:13:25	60	PC2 peak (ANU)	+150	McGregor, priv. comm.
		07:16:20	20	ME start (Okayama, 2.2 μm)	+345	Takeuchi *et al.* 1995
		07:16:45	15	ME start (AAT)	+355	Meadows *et al.* 1995
		07:17:02	30	ME start (ANU)	+372	McGregor, priv. comm.
		[illegible]		ME start (HST?)		
D	7	11:54:30	30	PC2 peak (ANU)	+120	McGregor, priv. comm.
		11:54:39	180	PC2 peak (AAT)	+126	Meadows *et al.* 1995
		11:58:30	30	ME start (ANU)	+360	McGregor, priv. comm.
		12:00:30	180	ME start (AAT)	+480	Meadows *et al.* 1995
		12:00:48	45	ME start (SPIREX)	+498	Sivaramakrishnan, priv. comm.
E	7	15:26:5	30	ME start (SAAO)	+314	Sekiguchi, priv. comm.
		[illegible]	0	ME start (SPIREX)	+960	Sivarsan, priv. comm.
		[illegible]	5	ME start (Calar Alto 2.2 μm)	+276	Herbst *et al.* 1995
		[illegible]	5	HST—Plume in sunlight (888 nm)	+471	Hammel *et al.* 1995
F	18			No impact observations reported		

Table 1: *Compilation of times of selected impact phenomena.* The column entitled $T - T_*$ gives the event times relative to the accepted impact times, which appear in Table 5.

Imp	Date	Time (UT)	± (s)	Event[a]	$T - T_*$ (s)	Reference
G	18	07:32:20	30	PC1 start (ANU)	− 73	McGregor, priv. comm.
		07:32:58	180	PC1 start (AAT)	− 35	Meadows *et al.* 1995
		07:33:31	15	HST—Bright pixels (888 nm)	− 2	Hammel *et al.* 1995
		07:33:33	5	Galileo PPR peak (945 nm)	0	Martin *et al.* 1995
		07:33:37	5	Galileo NIMS start (1.5 μm)	+ 4	Carlson *et al.* 1995a
		07:34:32	30	PC2 start (SPIREX)	+ 59	Severson, priv. comm.
		07:34:43	30	PC2 start (ANU)	+ 70	McGregor, priv. comm.
		07:35:24	8	HST—Emission in shadow (888 nm)	+111	Hammel *et al.* 1995
		07:35:30	30	PC2 peak (ANU)	+117	McGregor, priv. comm.
		07:35:59	180	PC2 (AAT)	+127	Meadows priv. comm.
		07:38:24	8	HST—Plume in sunlight, 953	+291	Hammel *et al.* 1995
		07:39:20	30	V5 start (ANU)	+357	McGregor, priv. comm.
		07:39:37	30	V5 start (SPIREX)	+367	Severson, priv. comm.
		07:39:47	8	[illegible]	+377	[illegible]
		[illegible]	[illegible]	V5 start (AAT)	+413	Meadows priv. comm.
		19:31:45	20	PC1 peak (Calar Alto 2.3 μm)	− 14	Hamilton *et al.* 1995
		19:31:46	4	PC1 peak (Pic du Midi 2.3 μm)	− 12	Colas *et al.* 1995
		19:31:50	4	Galileo PPR peak (945 nm)	− 8	Martin *et al.* 1995
		19:32:30	4	PC2 start (Calar Alto 2.3 μm)	+ 32	Tozzi *et al.* 1995
		19:32:41	2	PC2 start (Pic du Midi 2.3 μm)	+ 42	Colas *et al.* 1995
		19:32:47	2	PC2 start (Calar Alto 2.3 μm)	+ 48	Hamilton *et al.* 1995
		19:32:57	2	PC2 start (Pic du Midi 2.3 μm)	+ 58	Brahic expedition team
		19:33:05	2	PC2 peak (Pic du Midi 2.3 μm)	+ 67	Colas *et al.* 1995
		19:33:16	4	PC2 peak (Calar Alto 2.3 μm)	+ 78	Tozzi *et al.* 1995
		19:37:25	2	V5 start (Pic du Midi 2.3 μm)	+326	Colas *et al.* 1995
		19:37:27	3	V5 start (Calar Alto 2.3 μm)	+328	Hamilton *et al.* 1995
		19:37:35		V5 start (Calar Alto 2.3 μm)	+336	Tozzi *et al.* 1995
G				No impact observations reported		

Table 1: *Continued*

Imp	Date	Time (UT)	± (s)	Event*	$T - T_*$ (s)	Reference
K	19	10:20:41	30	Leader start (ANU)	216	McGregor, priv. comm.
		10:22:42	40	Leader start (AAT)	- 95	Meadows *et al.* 1995
		10:23:03	30	PC1 start (ANU)	- 74	McGregor, priv. comm.
		10:23:19	40	PC1 start (AAT)	- 58	Meadows priv. comm.
		10:23:57	40	PC1 peak (AAT)	- 20	Meadows priv. comm.
		10:24:03	5	PC1 peak (Okayama, 2.3 μm)	- 14	Watanabe *et al.* 1995
		10:24:17	2	Galileo SSI peak (890 nm)	0	Chapman *et al.* 1995
		10:25:03	5	PC2 start (Okayama, 2.3 μm)	+ 46	Watanabe *et al.* 1995
		10:25:24	30	PC2 start (ANU)	+ 67	McGregor, priv. comm.
		10:25:26	5	PC2 peak (Okayama, 2.3 μm)	+ 69	Watanabe *et al.* 1995
		10:25:30	20	PC2 peak (ANU)	+ 73	McGregor, priv. comm.
		10:30:23	5	ME start (Okayama, 2.3 μm)	+366	Watanabe *et al.* 1995
		10:30:29	20	ME start (ANU)	+372	McGregor, priv. comm.
		22:16:55		PC1 start (Calar Alto 2.3 μm)	-31	Hamilton *et al.* 1995
		22:17:41	3	PC1 peak (Calar Alto 2.3 μm)	9	Hamilton *et al.* 1995
		[illegible]	[illegible]	[illegible]	[illegible]	[illegible]
		22:17:27	2	PC2 start (Calar Alto 2.3 μm)	+ 38	Hamilton *et al.* 1995
		22:17:29	5	PC2 start (Pic du Midi 2.1 μm)	+ 40	Cobos *et al.* 1995
		22:17:49	2	PC2 start (La Palma 2.2 μm)	+ 57	Lagage *et al.* 1995
		22:17:59	5	PC2 peak (Pic du Midi 2.1 μm)	+ 69	Cobos *et al.* 1995
		22:22	60	ME start (Calar Alto 2.3 μm)	+311	Hamilton *et al.* 1995
		22:22:55	8	ME start (Pic du Midi 2.1 μm)	+366	Cobos *et al.* 1995
V	20	06:08	60	ME? start (Keck)	+260	de Pater, priv. comm.
N	20	10:20:20	2	Galileo SSI peak (890 nm)	0	Chapman *et al.* 1995
		10:35:42	30	ME start (ANU)	+382	McGregor, priv. comm.
Z	20			No impact observations reported		
P1	20			No impact observations reported		

Table 1: Continued

Imp	Date	Time (UT)	± (s)	Event*	$T - T_0$ (s)	Reference
Q2	20	19:44		PC2? start (Pic du Midi 2.1 μm)	0	Email exploder report
		19:44:10	1	PC2? start (Calar Alto 3.1 μm)	+ 10	Tozzi *et al.* 1995
		19:44:40	1	PC2? peak (Calar Alto 3.1 μm)	+ 40	Tozzi *et al.* 1995
		19:44:47	3	PC2? start (Calar Alto 2.3 μm)	+ 47	Herbst *et al.* 1995
		19:52:10	1	ME start (Calar Alto 3.1 μm)	+490	Tozzi *et al.* 1995
		19:52:24	15	ME start (Calar Alto 2.3 μm)	+504	Herbst *et al.* 1995
Q1	20	20:09:50	1	PC0 start (Calar Alto 3.1 μm)	243	Tozzi *et al.* 1995
		20:10:30	1	PC0 peak (Calar Alto 3.1 μm)	283	Tozzi *et al.* 1995
		20:13	1	PC1 (Pic du Midi 2.1 μm)	3[illegible]	Email exploder report
		20:13:15	[illegible]	PC1 start (Calar Alto 3.1 μm)	5[illegible]	Tozzi *et al.* 1995
		20:13:[illegible]	[illegible]	PC1 start (Calar Alto 2.3 μm)	3[illegible]	Herbst *et al.* 1995
		20:13:40	[illegible]	PC1 peak (Calar Alto 3.1 μm)	3[illegible]	Tozzi *et al.* 1995
		20:13:[illegible]	[illegible]	Galileo EPD peak (2-5 μm)	3[illegible]	Mueller *et al.* 1995
		20:13:[illegible]	[illegible]	PC2 start (Calar Alto 3.1 μm)	+2[illegible]7	Tozzi *et al.* 1995
		[illegible]	[illegible]	PC2 peak (Calar Alto 3.1 μm)	+2[illegible]7	Tozzi *et al.* 1995
		20:[illegible]	[illegible]	ME start (Calar Alto 3.1 μm)	3[illegible]2	Tozzi *et al.* 1995
		20:19:47	[illegible]	ME start (Calar Alto 2.3 μm)	[illegible]	[illegible]
R	21	05:34:32	180	PC1 start (AAT)	− 25	Meadows priv. comm.
		05:34:[illegible]	8	PC1 start (Keck 2.3 μm)	− 13	Graham *et al.* 1995
		05:34:52	10	PC1 peak (Palomar 4.5 μm)	− 5	Nicholson *et al.* 1995
		05:34:52	8	PC1 peak (Keck 2.3 μm)	− 5	Graham *et al.* 1995
		05:35:08	22	Galileo NIMS start (3-5 μm)	+ 11	Carlson *et al.* 1995b
		05:35:27	10	PC2 start (Palomar 4.5 μm)	+ 30	Nicholson *et al.* 1995
		05:35:[illegible]	8	PC2 start (Keck 2.3 μm)	+ 49	Graham *et al.* 1995
		05:35:38	10	PC2 peak (Palomar 4.5 μm)	+ 51	Nicholson *et al.* 1995
		05:35:57	8	PC2 peak (Keck 2.3 μm)	+ 57	Graham *et al.* 1995
		05:38:34	30	ME start (Palomar 3.2 μm)	+217	Nicholson *et al.* 1995
		05:39:[illegible]	10	ME start (Palomar 4.5 μm)	+222	Nicholson *et al.* 1995
		05:[illegible]	30	ME start (ANU)	+303	McGregor, priv. comm.
		05:40:57	8	ME start (Keck 2.3 μm)	+260	Graham *et al.* 1995
		05:41:00	11	Galileo splash start (NIMS)	+363	Carlson *et al.* 1995b
		05:42:22	180	ME start (AAT)	+445	Meadows *et al.* 1995

Table 1 *Continued*

Imp	Date	Time (UT)	± (s)	Event[a]	$T - T_*$ (s)	Reference
S	21	15:17:36	30	PC2 peak (SAAO)	+ 66	Sekiguchi, priv. comm.
		15:19:20		PC2 start (Vainu Bappu, 1.65 μm)	+170	Bhatt 1994
		15:22	120	ME start (Calar Alto 2.3 μm)	+330	Herbst *et al.* 1995
		15:22:40	30	ME start (SAAO)	+370	Sekiguchi, priv. comm.
T	21			No impact observations reported		
U	21	22:00:37		ME? start (McDonald)	+ 25	Covington, priv. comm.
V	22	[illegible]	[illegible]	[illegible]	[illegible]	Nicholson, IAU pc
		[illegible]	[illegible]	[illegible]	[illegible]	Nicholson *et al.* 1995
W	22	[illegible]	[illegible]	[illegible]	[illegible]	Hamanowa *et al.* 1995
		08:06:24	20	PC2 start (ANU)	+ 8	McGregor, priv. comm.
		08:06:54	180	PC2 start (AAT)	+ 38	Nicholson, priv. comm.
		08:07:10	20	PC2 peak (ANU)	+ 54	McGregor, priv. comm.
		[illegible]	[illegible]	[illegible]	[illegible]	Hammel *et al.* 1995
		08:12:00	30	ME start (ANU)	+314	McGregor, priv. comm.
		[illegible]	[illegible]	[illegible]	[illegible]	Nicholson *et al.* 1995

[a] Key to abbreviations: AAT, Anglo-Australian Telescope, Mount Stromlo and Siding Spring Observatories, ANU, Australian National University, Mount Stromlo and Siding Spring Observatories, MSSSO, Multiple Space Telescope, now NASA Infrared Telescope Facility, Mauna Kea, Hawaii, Vainu Bappu Observatory, VBO, Vainu Bappu Telescope, SAAO, South African Astronomical Observatory, Sutherland, South Africa.

Table *Concluded*

• Impact Q2: We have assumed the precursor observed at Calar Alto was PC2. If it was PC1, the estimated impact time would be ∼ 1 minute later. Either way, the main event starts later than expected, possibly because it was very faint, and its real onset was below the limits of detectability.

• Impact Q1: A total of three precursors were seen from Calar Alto in the 3.1 μm band (Tozzi *et al.* 1995). Only one of these (PC1) fits the expected pattern relative to the main event start time; the others have been labeled PC0 and PC3 in the table, and remain unexplained.

• Impact R: Although Galileo NIMS data are available for this impact, they cannot be used to constrain the impact time very precisely, because the sampling time was large (∼ 11 s), and the sample nearest the impact time was missed (Carlson *et al.* 1995b). We adopt the impact time derived by Sekanina (this volume) using the ground-based IR light curves.

• Impact U: A possible detection is listed for this impact. It is not clear why larger telescopes, observing at the same time under excellent conditions, did not see the event. The reported time is consistent with the impact time derived from our final orbital solution, which is the time we adopt.

• Impact V: Light curves displayed only a short flash, which had the appearance of a faint first precursor; no main event was seen. The V fragment may have been too small to produce a plume or main event.

4. Post-impact improvements to the orbit solutions

In order to obtain the most accurate possible final estimates of the impact parameters, it was necessary to refine the orbit solutions from which they were computed. The most important improvement needed was to make the orbit solutions consistent with the observed impact times. If the solutions could be updated to "predict" the correct impact times, estimates of other parameters such as the impact locations would also become more accurate. Although the update could have been accomplished by making the impact time a constraint and forcing the orbit solution to satisfy it exactly, a better approach was simply to use the impact time as an additional measurement in the solution process. Accordingly, we augmented our orbit determination software to handle an impact time as a new measurement type. The new measurements were assigned conservative uncertainties – typically 5 s (1-sigma) for the impacts observed by Galileo, and 60 s or larger for fragments with impact times inferred from ground-based observations. We also modified our definition of impact oblivity, raising it up to the 10 bar level of Jupiter's atmosphere as defined by Lindal *et al.* (1981), but this change made little difference in the final solutions.

Using the impact times as measurements now, we computed new orbital solutions for the 16 fragments with observed impact phenomena. As an additional refinement, the planetary ephemeris was updated to the more accurate DE403 (Standish 1995, private communication). As a check, impact times were "predicted" from the new solutions; as expected, they matched the accepted times to within the assigned uncertainties. The systematic 7-minute error had been eliminated, at least for the 16 fragments whose impacts were observed. Significantly, the inclusion of the impact time in the orbit solutions did not adversely affect the residuals for the remaining observations. Typically, they increased by less than 0.1 arcsec over the entire observation span, although the differences ranged as high as 0.3 arcsec for some fragments. The largest changes in residuals were nearest impact. Clearly, systematic star catalog errors did not have to be very large to cause the observed 7-minute error in our predicted impact times. Assuming the catalog

Fragment	Data Interval	Number of Obs	Impact Obs.	Weighted rms (″)	Orbit Ref.
A	93 March 27–94 July 12.0	54	Y	0.22	A38
B	93 March 27–94 July 12.9	75	Y	0.29	B34
C	93 March 27–94 July 11.0	82	Y	0.19	C28
D	93 March 27–94 July 13.9	63	Y	0.21	D29
E	93 March 27–94 July 13.6	193	Y	0.20	E50
F	93 March 27–94 July 11.9	120	N	0.19	F33
G	93 March 27–94 July 13.8	168	Y	0.18	G52
H	93 March 27–94 July 13.9	172	Y	0.18	H43
K	93 March 27–94 July 14.0	83	Y	0.16	K45
L	93 March 27–94 July 10.0	139	Y	0.20	L49
N	93 March 27–94 July 11.1	63	Y	0.19	N36
P2	93 March 27–94 July 19.2	107	N	0.19	P37
P1	93 July 1–94 June 17.0	35	N	0.21	PA6
Q2	93 March 31–94 July 20.0	19	Y	0.10	QB13
Q1	93 March 27–94 July 19.2	163	Y	0.21	Q63
R	93 March 27–94 July 19.0	85	Y	0.22	R58
S	93 March 27–94 July 19.1	129	Y	0.23	S62
T	93 March 27–94 July 15.8	35	N	0.25	T22
U	93 March 27–94 July 7.1	26	N	0.29	U24
V	93 March 27–94 July 19.0	55	Y	0.23	V27
W	93 March 27–94 July 16.1	80	Y	0.26	W52

Table 2. Summary of orbit solutions. The data interval indicates the dates of the first and last observations used in the solutions, excluding the impact observation. The number of observations similarly excludes the impact observation. The following column indicates whether the impact time was used as an observation in the solution. The final two columns give the weighted rms residual and the orbit reference identifier.

errors were the culprit, the new residuals were now a better representation of the actual measurement errors. In other words, the inclusion of the impact time had moved at least a portion of the star catalog errors out of the orbit solution into the residuals, where they belong. A small effect on the predicted 1992 perijove distances was also noted: the new solutions lowered them by ≈ 500 km.

The inclusion of impact times was a powerful method for improving orbit solutions, but it was applicable only to fragments whose impacts were observed. How could the orbit solutions for the other fragments be improved as well? One possible technique was simply to add an empirical 7-minute correction to the predicted impact times for those fragments, and use these as pseudo impact times when computing new solutions. But this was rather *ad hoc*. The approach we adopted was to improve orbit solutions by improving the measurements upon which the solutions were based.

Observers typically captured several fragments in each of their astrometric images, and reduced the positions of all the fragments using the same stars. Our technique took advantage of the fact that errors in the star positions produced the same measurement bias for all fragments in a given observation set. (An 'observation set' is the set of individual fragment measurements made from a single astrometric image and reduced together, presumably relative to a single set of reference stars.) The measurement bias can be seen clearly in a plot of the fragment residuals in a given set. The residuals typically cluster around a point offset from the origin by a few tenths of an arc second,

	e	q (AU)	ω (deg)	Ω (deg)	i (deg)	T_p (1994 TDB)
A	0.21620917	5.38056310	354.89352	22.537655	6.003294	Mar. 24.10320
B	0.21561980	5.38065243	354.90067	22.565286	5.990216	Mar. 24.52991
C	0.21516872	5.3s04114'1	354.90826	22.581389	5.981965	Mar. 24.81127
D	0.21472534	5.38036971	354.91311	22.600306	5.972968	Mar. 25.10038
E	0.21411065	5.38031878	354.91617	22.613781	5.966629	Mar. 25.30070
F	().21358484	5,38036243	354.93314	22.651606	5.948163	Mar. 25.96840
G	0.2128S148	5.38011243	354.93119	22.680082	5.935514	Mar. 26.32445
H	0.21177932	5.37997339	354.93843	22.728309	5.912868	Mar. 27.08466
K	0.2101? 545	5.37977493	354.96756	22.788975	5.885070	Mar. 28.05310
L	0.20936108	5.379631"/1	354.98153	22.837514	5.863131	Mar. 28.84854
N	().2()827689	5.37953629	354.99095	22.886270	5.840458	Mar. 29.63418
P2	0.20788730	5.37960765	355.00194	22.904724	5.831257	Mar. 30.00933
P1	0.20774507	5.37968923	354.99928	22.909078	5.829288	Mar. 29.92297
Q2	0.20745337	5.37940298	355.01104	22.924560	5.823607	Mar. 30.23482
Q1	0.20710426	5.37934828	355.01109	22.927985	5.822819	Mar. 30.27142
R	0.20658149	.5.37923176	355.02279	22.966459	5.805868	Mar. 30.87835
S	0.20573678	5.37912911	355.03335	22.006655	5.788483	Mar. 31.50154
T	0.20550407	5.37931862	355.03349	22.016204	5.783002	Mar. 31.63843
U	0.20516743	5.37914092	355.04114	22.034174	5.776310	Mar. 31.94118
V	0.20461625	5.37904612	355.05809	22.060787	5.764890	Apr. 1.37239
W	0.20.428226	5.37890776	355.05511	22.077213	5.758370	Apr. 1.63988

Table 3. Osculating **heliocentric** orbital elements for the fragments of comet Shoemaker-Levy 9 at epoch 1994 May 8.0 TDB = JD 2449480.5 TDB. The elements are eccentricity (e), perihelion distance (q), argument of perihelion (ω) longitude of the ascending node (Ω), inclination (i), and time of perihelion passage (T_p). The angular orbital elements are referred to the ecliptic plane and equinox of J2000.

with a scatter much smaller than the bias. We concluded that the bias was mostly due to star catalog errors, while the scatter was mostly due to the actual errors of measurement.

When looking at residuals, we concentrated on the six fragments with the most accurate orbit solutions, G, H, K, L, Q, and W, which we called the *primary* fragments. These had the largest astrometric data sets and impact times known to within a few seconds from Galileo observations. Almost all of the 37 observation sets contained at least one primary fragment, and most contained several. Residuals for the primary fragments typically clustered around the bias point with a scatter smaller than that of the other residuals. Our estimate of the measurement bias of each observation set was obtained by averaging the residuals of the *primary fragments*. We then subtracted this bias from all measurements in the set to obtain corrected 'synthetic' observations. The measurements in each set were assigned a single noise value according to the scatter of the residuals. Because biases had been removed, most noise values were much smaller than in previous solutions, typically 0.2 arcsec for high quality observations.

To test this method, we applied it to individual *primary fragments* to see whether we could correctly predict the impact times. For example, to test the method on fragment G, we computed observation biases by averaging the residuals of the other primary fragments, adjusted the G observations by subtracting off the biases, and computed the synthetic solution *without using the G impact time as an observation*. The impact times predicted by these test solutions were very close to the accepted times, within 30 s in most cases, giving us confidence that our approach could predict accurate impact times even for those fragments whose impacts were not observed.

	e	q (km)	ω (deg)	Ω (deg)	i (deg)	T_p (1994 TDB)
A	0.99860178	37359.28	43.224821	28.754106	88.510529	July 16.98246
B	0.99859179	37635.83	43.245621	28.722794	87.742186	July 17.26248
C	0.99860684	37238.92	43.218521	28.732690	88.799176	July 17.44353
D	0.99860765	**37223.01**	43.219367	28.710416	88.776404	July 17.64044
E	0.99860837	37208.32	43.220157	28.704456	88.875632	July 17.77938
F	0.99860544	**37300.4s**	43.222927	28.746587	88.280449	July 18.17450
G	**0.99861241**	**37121.95**	43.214139	28.753708	89.136959	July 18.46555
H	0.9986]664	**37024.28**	43.212373	28.768492	89.256703	July 18.96760
K	0.99862089	36930.22	43.209959	28.784875	89.585060	July 19.59097
L	0,99862481	36841.23	43.209.20[illegible]	28.778211	89.785022	July 20.08892
N	().99863152	36676.73	43.209210	28.807826	89.601233	July 20.60125
J'2	0.99863451	36604.26	43.213514	28.752492	89.013508	July 20.80606
1'1	0.99863423	36611.50	43.213503	28.758538	88.212721	July 20.85685
Q?	0.99S63402	36621.70	43.208360	28.726438	89.832856	July 20.98913
Q]	0.99862993	36731.86	43.208967	28.730548	90.150681	July 21.00939
R	0.99863325	36655.41	43.209414	28.739518	90.261716	July 21.40164
s	**0.99s63588**	36598.27	43.210767	28.752323	90.278231	July 21.80819
T	0.99.864005	364/39.40	43.215562	28.766900	88.935962	July 21.93115
U	0.99s63734	36567.67	43.208609	28.728497	89.832581	July 22.09104
V	0.99s63940	36521.02	43.208274	28.795726	90.006578	July 22.35899
W	0.99s63886	36538.68	43.212649	28.774798	90.611633	July 22.51406

Table 4. Osculating **jovicentric** orbital elements for the fragments of comet Shoemaker-Levy 9 at epoch 1994 May 8.0 TDB = JD 2449480.5 TDB. The elements are eccentricity (e), perijove distance (q), argument of perijove (ω), longitude of the ascending node (Ω), inclination (i), and time of perijove passage (T_p). The angular elements are referred to the ecliptic plane and equinox of J2000.

Our final set of orbit solutions were computed using the synthetic method just described, with impact times used as observations when available. Table 2 summarizes these solutions, giving for each fragment the data interval, number of observations, the weighted rms residual, an indication of whether we used the impact time as an observation, and our orbit reference identifier. The final orbital elements themselves are given in heliocentric form in Table 3, and jovicentric form in Table 4. An independent orbit solution for fragment P1 is included for the first time. The extremely small weighted rms residuals for these solutions, less than 0.2 arcsec for half of the solutions, and less than 0.3 arcsec for the rest, is due to the removal of the measurement biases. The attentive reader may note that our data interval for fragment Q2 begins on March 3^{d}, 1993, well before Q2 was seen on its own. We have used the Q1 position on this date as a pseudo-measurement to constrain the Q2 solution because this was approximately the time Q2 split away from Q1 (Sekanina 1995).

It is interesting to integrate the orbit solutions backward to the 1992 perijove to see how closely the fragments come together. Figure 2 shows the clustering of the 1992 perijove times and perijove distances. Only certain fragments are included, as off-train fragments presumably split well after perijove. The perijove times all fall within a 45-minute period, and the perijove distances within a 500-km range. The inter-fragment distances themselves are quite large, however, because of the dispersion in the perijove times.

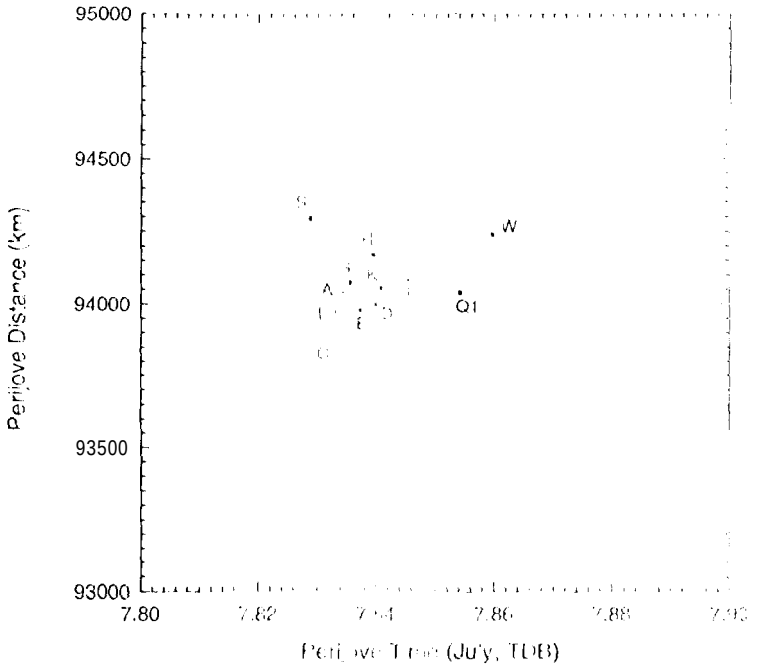

Figure 2. Plot of 1992 perijove distance vs. perijove times of our final orbit solutions for 12 on-train fragments. Even though the solutions have not been constrained to come together at this perijove, they do cluster fairly well. The perijove times, shown as day and fraction of day in July 1992, all fall within a 45 minute period.

5. Summary of impact times, impact locations, and impact geometries

Our final estimates of the impact times and locations of the fragments of SL9 are given in Table 5. The estimated impact times in this table are slight revisions to earlier estimates compiled at IAU Colloquium 156. Impact was defined to occur at the 100-mbar level of Jupiter's atmosphere. The impact estimates for all fragments except J and M are based on the independent orbit solutions discussed in the previous section. The estimates for the 'lost' fragments J and M were obtained by applying our tidal disruption model to the orbit for fragment Q1 and matching the astrometry of these two fragments relative to Q1. The third column of Table 5 contains our final pre-impact prediction for each of the fragments, taken from the set of predictions we distributed electronically on the UMD e-mail exploder. The fourth column lists our final best estimates, which were inferred directly from impact phenomena for 12 fragments, as described in section 3, and computed from the orbit solutions for the rest. All times are as viewed from the Earth, and therefore include the light travel time. The impact time uncertainties are rough estimates which indicate our confidence level in the accepted time; they are not formal 1-sigma uncertainties. The impact latitude is jovicentric, while the longitude is System III, measured westwards on the planet. The meridian angle is the jovicentric longitude of the impact point measured from the midnight meridian towards the morning terminator. At the latitude of the impacts, the limb as viewed from the Earth is at meridian angle 76 deg, and the terminator is at meridian angle 87 deg.

The final column of Table 5 gives the angular distance of the impacts behind the limb, a more useful parameter than the Earth-Jupiter-fragment (E-J-F) angle we gave in our

Event	Impact Time (UTC)			Impact Location		Merid.	Ang. Dist.
	Date (July)	Predicted h m s	Accepted h m s	Lat. deg	Lon (deg)	Angle (deg)	Behind Limb (deg)
A	16	19:59:40	20:10:30	-43.35	18	65.40	7.7
B	17	02:54:13	02:50:00	-43.22	67	63.92	8.8
C	17	07:02:14	07:10:50	-43.47	22	66.11	7.1
D	17	11:47:00	11:52:30	-43.53	3	66.16	7.1
E	17	15:05:31	15:11:40	-43.51	152	66.40	6.9
F	18	00:29:21	00:35:45	-43.68	135	65.30	7.7
G	18	07:28:32	07:33:33	-43.66	26	67.09	6.4
H	18	19:25:53	19:31:59	-43.79	99	67.45	6.1
J	19	02:40	01:35	-43.75	~ 316	68.05	~6
K	19	10:18:32	10:24:17	-43.86	278	68.32	5.5
L	19	22:08:53	22:16:49	-43.96	348	68.86	5.1
M	20	05:45	06:00	-43.93	~ 261	69.25	~5
N	20	10:20:02	10:29:20	-44.31	71	68.68	5.1
P2	20	15:16:20	15:21:11	-44.69	249	67.58	5.8
P1	20	16:30	16:32:35	-45.02	~ 293	65.96	6.9
Q2	20	19:47:11	19:44:00	-44.32	46	69.26	4.7
Q1	20	20:04:09	20:13:53	-44.00	63	69.85	4.3
R	21	05:28:50	05:31:57	-44.10	42	70.21	4.1
S	21	15:12:49	15:16:30	-44.22	33	70.31	4.0
T	21	18:03:45	18:09:56	-45.01	143	67.73	5.7
U	21	21:48:30	22:00:02	-44.48	278	69.54	4.5
V	22	04:16:53	04:23:20	-44.47	149	69.96	4.2
W	22	17:59:45	08:06:16	-44.13	283	71.29	3.4

Table 5. Summary of impact times and locations

earlier sets of predictions. The use of the E-J-P angle has led to a small error in computing the precise distance of the impact behind the limb. Because of Jupiter's oblateness, the limb of Jupiter cannot be assumed to be located at an E-J-P angle of 90 deg. In fact, at the latitude of the impacts, the limb was at an E-J-P angle of ~ 90.3 deg, moving the impacts a little closer to the limb than previously thought. Our final estimates put impact W less than 3.5 deg behind the limb.

Table 6 summarizes the impact velocities and directions as computed from our final orbit solutions. These parameters are all related to the velocity of the fragment relative to the impact point in a frame rotating with Jupiter at the System III rotation rate. Thus, the relative velocity includes a small component due to Jupiter's rotation. The incidence angle is measured from the local vertical, while the azimuth angle is measured from north towards the west.

6. Pre-breakup orbital history

Backward numerical integrations of SL9's orbital motion can provide clues as to the nature and origin of the object. Accurate knowledge of the comet's pre-breakup motion is essential in searches for the progenitor comet in existing image libraries. A pre-breakup detection would enable limits to be set on the size of the progenitor nucleus, and even a non-detection is useful, if we could be sure of the ephemeris. Tancredi *et al.* (1993) reported that they did not see the comet in a 30-min exposure of the Jupiter region taken in March 1992, which had a limiting magnitude of 21.3. The investigation of SL9's pre-breakup motion also helps determine when the comet was likely captured by Jupiter,

Event	Velocity (km s^{-1})	Incidence Angle (deg)	Azimuth Angle (deg)
A	61.23	33.3	14.37
B	61.32	33.2	13.34
C	61.29	33.2	14.89
D	61.29	33.2	14.91
E	61.31	33.2	15.08
F	61.23	33.1	14.33
G	61.36	33.2	15.59
H	61.39	33.2	15.86
K	61.46	33.2	16.48
L	61.50	33.1	16.86
N	61.48	33.0	16.73
P2	61.40	32.7	15.93
P1	61.28	32.6	14.77
Q2	61.53	33.0	17.15
Q1	61.57	33.2	17.59
R	61.60	33.1	17.8
S	61.61	33.1	17.96
T	61.41	32.5	16.06
U	61.55	32.9	17.38
V	61.58	32.9	17.69
W	61.68	33.2	18.57

Table 6. Summary of impact velocities and directions

and provides insight into the object's pre-capture heliocentric orbit. Unfortunately, SL9's orbit about Jupiter was among the most chaotic of any known solar system body, with an effective Lyapunov time on the order of 10 years (Benner and McKinnon 1995). As a result, a single backward numerical integration does not provide definitive answers on the orbital history of this object. A better approach is to account for the uncertainties in the initial conditions of the backward integrations, and to investigate the motion in a statistical manner using a Monte Carlo analysis (Chodas and Yeomans 1995).

The first difficulty encountered when investigating SL9's pre-breakup orbital history is how to solve the Humpty-Dumpty problem, i.e., how to obtain the orbit for the progenitor nucleus from the orbits of the fragments. Our solution to this problem was simply to assume that fragment K was near the center of mass of the original nucleus, and that its motion was unaffected by the breakup. As initial conditions for the progenitor nucleus, we used our orbit solution for fragment K, along with the actual orbit uncertainties and their correlations. Fragment K was a natural choice, since it was closest to the mid-point of the train. We repeated our analyses with fragment L, which was also close to the mid-point, and obtained essentially the same results.

Our approach was to create a random ensemble of 1000 initial conditions whose statistics matched the actual orbital element uncertainties and correlations. Effectively, a six-dimensional uncertainty ellipsoid in orbital element space was populated with 1000 random points to obtain an ensemble of initial conditions consistent with the actual 6×6 covariance matrix of the orbital solution. As before, our dynamic model included solar and planetary perturbations, as well as perturbations from the Galilean satellites and Jupiter's oblateness (J2 and J4 terms).

Each sample point was integrated backward in time until it escaped from Jupiter, at which point its heliocentric orbital elements were tabulated. Orbits which had encounters

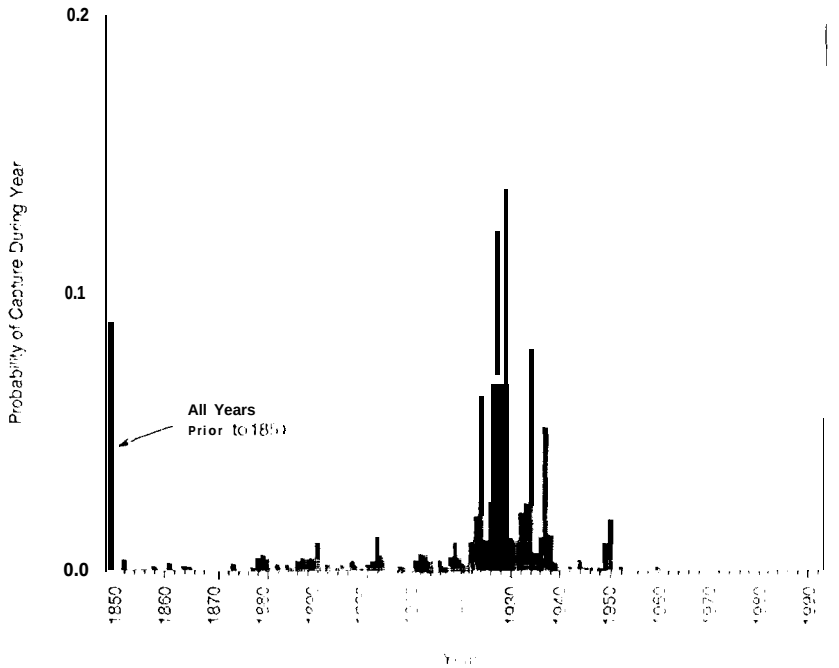

Figure 3. Histogram showing the probability that SL9 was captured in any given year back to 1850, based on a Monte Carlo analysis of 93 sample points. The most likely time of capture is 1929 ± 9 years (72% probability).

with Jupiter closer than that in 1992 were discarded. Escape was defined to occur when the jovicentric eccentricity exceeded unity and the distance from Jupiter exceeded 0.7 AU. Of course, the moment of escape in the backward integration is really the moment of capture when viewed in the forward direction.

Figure 3 shows a histogram of the number of samples which escaped from Jupiter each year back to 1850, when our integrations stopped. Nine percent of the samples were still in Jupiter orbit at the end of integrations. The most likely time of capture, with a probability of 72%, was 1929 ± 9 years. During its several-decade residency as a captured comet, SL9 orbited Jupiter with a period of 2.3 years and a semi-major axis of ≈ 0.2 AU. Its orbit was highly inclined to Jupiter's equator and oscillated between periods of near-circularity and periods of high eccentricity. Throughout this time, the comet remained within four degrees of Jupiter, as viewed from the Earth. Its pre-discovery ephemeris is fairly well-determined, at least as far back as 1970, and the ephemeris uncertainties grow to no more than 0.25 degree (1-sigma) during this time. Figure 4 shows a representative trajectory for the captured comet in a rotating, jovicentric frame, following the comet from capture in 1928 to the comet's final orbit in 1992–1994. Although in this example the comet was captured from the direction of the Sun, other cases show the comet being pulled in from the anti-solar direction. Comets are typically captured as they pass near the libration points on the Jupiter-Sun line.

The pre-capture heliocentric orbits of our samples were all of low inclination ($i < 6$ deg) and moderately low eccentricity ($e < 0.4$). As shown in Fig. 5, the pre-capture orbits fell into two groups: those orbits well inside Jupiter's orbit, and those well outside. On the orbits interior to Jupiter's orbit, capture occurred at aphelion, while on those exterior, capture occurred at perihelion. None of the pre-capture orbits crossed Jupiter's orbit.

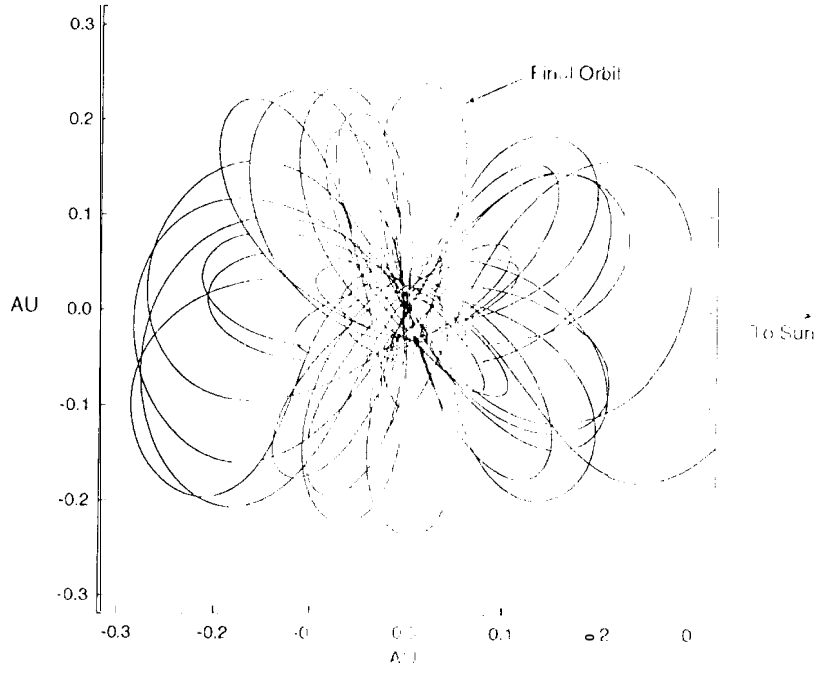

Figure 4. Orbital behavior of a representative trajectory for SL9, shown in a jovicentric rotating frame, and projected into the orbital plane of Jupiter. The comet enters the diagram from the solar direction in 1930, and completes 25 orbits about Jupiter before impact.

These findings are consistent with the general results of Carusi and Valsecchi (1979), and Kary and Dones (1995), who have shown that captures occur when minor bodies approach Jupiter along nearly-tangent orbits. In our analysis for SL9, capture from orbits interior to Jupiter's orbit was three times more likely than capture from orbits exterior to Jupiter's orbit. Benner and McKinnon (1995) obtained a similar result in their integrations for SL9, and noted that the preference for capture from interior orbits is really just a measure of the comparative ease with which captures (or escapes) occur at Jupiter's two libration points.

An important parameter used in classifying orbits of comets and asteroids is the Tisserand invariant with respect to Jupiter, T, which is approximately constant during encounters with the planet (Kresák 1979). The critical value of $T_o = 3$, where T_o is the value of T for $i = 0$, can be used to distinguish between cometary type orbits ($T_o < 3$) and asteroidal type orbits ($T_o > 3$). The Tisserand parameters for the samples in our analysis for SL9 straddled this boundary, with T_o values ranging from 2.99 to 3.04, and a mean of ~ 3.02, indicating that SL9's pre-capture orbit was probably asteroid-like. However, as noted by Benner and McKinnon (1995) the inner distribution of possible pre-capture orbits for SL9 overlaps a group of known comets, referred to as quasi-Hildas by Kresák. With Tisserand parameter values ranging from 3.00 to 3.01, these comets also have asteroid-like orbits. In fact, they occupy the same region in a/e phase space as the Hilda asteroids, although they are not in the same stable 3:2 resonances as the Hildas. Three members of the quasi-Hilda group, P/Gehrels 3, P/Shoemaker-Chernykh, and P/Helin-Roman-Crockett, and one former member, P/Oterma, are plotted in Fig. 5. They reside comfortably inside the inner distribution of possible SL9 orbits. P/Oterma made a close approach to Jupiter in 1963, moving to an orbit exterior to that of Jupiter,

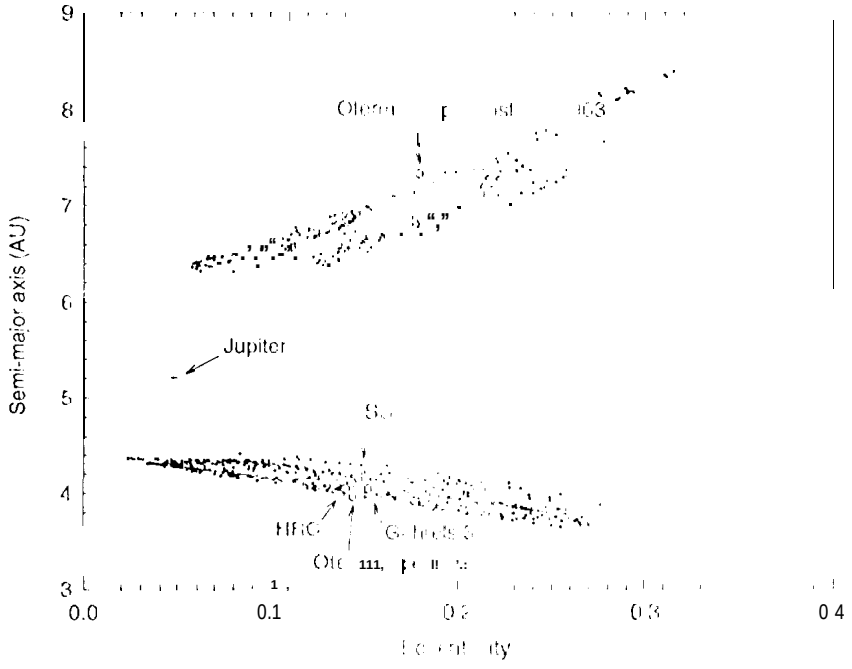

Figure 5. Scatter plot of ~ 850 possible pre-impact orbits for SL9. The orbits of four known comets are shown as open circles. SC denotes P/Shoemaker-Churyumov, and HRC denotes P/Helin-Roman-Crockett. P/Oterma's orbit is shown both before and after its 1963 close approach to Jupiter.

and now resides in the outer distribution of possible SL9 orbits. All four of these comets have either been temporarily captured by Jupiter in the past, or will be temporarily captured in the future (Yeomans and Chodas 1994b). Before its final capture, SL9 was probably also a member of this quasi-Hilda cometary group.

7. Summary and conclusions

This paper has reviewed the early orbit computation efforts for SL9, including the surprising discoveries that the comet was in orbit about Jupiter, and that it would impact the planet. We confirmed these results, and computed the probability of impact, which rose from 50% to near unity during the two week period after the impact announcement, as more astrometric measurements were added to the orbit solutions. We also determined that the impact of the center of the train would occur on the far side of the planet. After solar conjunction, and in the months leading up to the impacts, we computed increasingly accurate orbit solutions for the individual fragments, using the growing set of astrometric observations. Our predictions of the times and locations of the impacts were regularly made available to the astronomical community via the electronic bulletin board and e-mail exploder operated by the University of Maryland.

After the impacts, we estimated the actual impact times from the times of observed impact phenomena, which we have compiled in Table 1. Our final predicted impact times were systematically early by ~ 7 minutes, probably due to systematic errors in the reference star catalogs used in the reduction of the fragments' astrometric positions. We refined our orbit solutions by using the observed impact times as additional data for

16 of the fragments, and by estimating and removing star catalog errors from all the astrometric observations. Our final orbit solutions for 21 fragments are summarized in Table 2, and the heliocentric and jovicentric orbital elements are presented in Tables 3 and 4, respectively. Our best estimates of the impact times and impact locations are given in Table 5. Sixteen of the impact times were derived from the times of observed impact phenomena, while the remaining times were computed directly from the orbit solutions. The new estimates for the impact locations are 0.5–1 deg closer to the limb than in previous estimates.

We investigated the pre-breakup orbital history of SL9 by performing a Monte Carlo analysis of backward integrations, using an ensemble of orbits whose mean and covariance were consistent with our orbit solution for fragment K. We assumed that this fragment originated near the center of mass of the progenitor nucleus, and that its motion was unaffected by the breakup process. Our analysis showed that SL9 had been orbiting Jupiter for decades before its discovery, and that it was most likely captured from heliocentric orbit in 1929 ± 9 years. Prior to capture, SL9 was in a low-inclination, low-eccentricity heliocentric orbit, entirely inside Jupiter's orbit or, less likely, entirely outside. Its pre-capture orbit is consistent with a group of comets called the quasi-Hildas.

As a part of our investigation of SL9, we developed a number of new techniques with regard to cometary orbit determination. We successfully determined the probability of collision of a comet and a planet. We accurately predicted the times and locations of the impacts of the cometary fragments on Jupiter. Our orbit computations used not only planetary and solar perturbations, but also perturbations due to the Galilean satellites and Jupiter's oblateness. We included the observed Jupiter impact times as data in our post-impact orbit solutions, and successfully removed star catalog biases from the sets of astrometric data. To our knowledge, the dynamical modeling of this comet's motion is the most complex cometary orbit determination problem yet undertaken, and our resultant orbit solutions for the 21 fragments of comet Shoemaker-Levy 9 have the smallest rms residuals of any comet to date.

This work would not have been possible without the selfless contributions of the many observers who supplied astrometric data for SL9. We would also like to thank the many observers who provided us with the precise times of impact-related phenomena. Finally, we wish to thank Z. Sekanina and P. Nicholson for helpful comments and suggestions. This work was supported by the NASA Planetary Astronomy Program. The research was performed at the Jet Propulsion Laboratory, California Institute of Technology, under contract with the National Aeronautics and Space Administration. Support for this work was also provided by NASA through grant number GO-5624.03-93A from the Space Telescope Science Institute, which is operated by the Association of Universities for Research in Astronomy, Incorporated, under NASA contract NAS5-26555.

REFERENCES

Benner, L. A. M. & McKinnon, W. B. 1995 On the orbital evolution and origin of comet Shoemaker-Levy 9. Icarus **118**, 155–168.

Bhatt, H. C. 1994 IAU Circular 6039, Jul. 27.1994.

Boslough, M., Crawford, D., Robinson, A. & Trucano, T. 1994 Mass and penetration depth of Shoemaker-Levy 9 fragments from observed photometry. Geophys. Res. Lett. **21**, 1555.

Boslough, M., Crawford, D., Trucano, T. & Robinson, A. 1995 Numerical modeling of Shoemaker-Levy 9 impacts as a framework for interpreting observations. Geophys. Res. Lett. 22, 1821.

Campbell, J. K. & Synnott, S. P. 1985 Gravity field of the jovian system from Pioneer and Voyager tracking data. Astron. J. 90, 364–372.

Carlson, R. W., Weissman, P. R., Segura, M., Hui, J., Smythe, W. D., Johnson, T. V., Baines, K. H., Drossart, P., Encrenaz, T., Leader, J. R., & Herman, R. 1995a Galileo infrared observations of the Shoemaker-Levy 9 G impact fireball. A preliminary report. Geophys. Res. Lett. 22, 1561–1564.

Carlson, R. W., Weissman, P. R., Hui, J., Smythe, W. D., Baines, K. H., Johnson, T. V., Drossart, P., Encrenaz, T., Leader, J. R., Herman, R. 1995b Some timing and spectral aspects of the G and R collision events as observed by the Galileo near-infrared mapping spectrometer. In Proceedings of the European SL-9/Jupiter Workshop (eds. R. West and H. Bohnhardt) pp. 69–73. ESO.

Carusi, A., & Valsecchi, G. B. 1979 Numerical simulations of close encounters between Jupiter and minor planets. In Asteroids, (ed. T. Gehrels) pp. 391–416. University of Arizona Press.

Carusi, A., Kresak, L., Perozzi, E., Valsecchi, G. B. 1985 Long-term evolution of short-period comets. Adam Hilger Ltd.

Chapman, C. R., Merline, W. J., Klaasen, K., Johnson, T. V., Heffernan, C., Belton, M. J. S., Ingersoll, A. P., & the Galileo Imaging Team 1995 Preliminary results of Galileo direct imaging of S-L 9 impacts. Geophys. Res. Lett. 22, 1561.

Chodas, P. W. 1993 Estimating the impact probability of minor planet with the earth. Bull. Am. Astron. Soc. **25**, 1236.

Chodas, P. W., & Yeomans, D. K. 1993 The upcoming collision of comet Shoemaker-Levy 9 with Jupiter. Bull. Am. Astron. Soc. 25, 1042.

Chodas, P. W., & Yeomans, D. K. 1994a The impact of comet Shoemaker-Levy 9 with Jupiter. Bull. Am. Astron. Soc. 26, 1022.

Chodas, P. W., & Yeomans, D. K. 1994b Comet Shoemaker-Levy 9 impact times and impact geometries. Bull. Am. Astron. Soc. 26, 1069.

Chodas, P. W. & Yeomans, D. K. 1995 The pre-breakup orbital history of comet Shoemaker-Levy 9. Bull. Am. Astron. Soc. **27**, 1111.

Chodas, P. W., Yeomans, D. K., & Sekanina, Z. 1994 IAU Circular 5941 February 24, 1994.

Colas, F., Tiphene, D., Lecacheux, J., Dros, E., le Batz, B., Pau, S., Roman, D., & Sevre, F. 1995 Near infrared imaging of SL9 impacts on Jupiter from Pic-du-Midi observatory. Geophys. Res. Lett. 22, 1765–1768.

Davies, M. E., Abalakin, V. K., Brahic, A., Bursa, M., Chovitz, B. H., Lieske, J. H., Seidelmann, P. K., Sinclair, A. T., & Tjuflin, Y. S. 1992 Report of the IAU/IAG/COSPAR working group on cartographic coordinates and rotational elements of the planets and satellites: 1991. Cel. Mech. **53** 377–397.

de Pater, I., Graham, J., & Jernigan, G. 1994 IAU Circular 6024, July 17, 1994.

Graham, J. R., de Pater, I., Jernigan, J. G., Liu, M. C., Brown, M. E. 1995 The fragment R collision: W. M. Keck Telescope Observations of SL9. Science **267**, 1320–1325.

Hamilton, D. P., Herbst, T. M., Richichi, A., Bohnhardt, H., & Ortiz, J. L. 1995 Calar Alto observations of Shoemaker-Levy 9: Characteristics of the H and L impacts. Geophys. Res. Lett. **22**, 2417–2420.

Hammel, H. B., Beebe, R. F., Ingersoll, A. P., Orton, G. S., Mills, J. R., Simon, A. A., Chodas, P. W., Clarke, J. T., DeJong, E., Dowling, T. E., Harrington, J., Huber, L. F., Karkoschka, E., Santori, C. M., Toigo, A., Yeomans, D., & West, R. A. 1995 Hubble Space Telescope

imaging of Jupiter: atmospheric phenomena created by the impact of comet Shoemaker-Levy 9. Science **267,** 1288-1296.

Herbst, T. M., Hamilton, D. P., Bohnhardt, H., Ortiz Moreno, J. L. 1995 Near infrared imaging and spectroscopy of the SL-9 impacts from Calar Alto. Geophys. Res. Lett. **22,** 2413-2416.

Jewitt, D., Luu, J., & Chen, J. 1993 Physical properties of split comet Shoemaker-Levy 9. Bull. Am. Astron. Soc. **25,** 1042.

Kary, D. M., & Dones, L. 1995 Capture statistics of short-period comets: Implications for comet Shoemaker-Levy 9. Icarus, (submitted)

Kresák, L. 1979 Dynamical interrelations among comets and asteroids. In Asteroids, (ed. T. Gehrels). pp. 289-309. University of Arizona Press.

Lagage, P. O., Aldemard, P. H., Pantin, E., Jouan, R., Masse, P., Sauvage, M., Olofsson, G., Huldtgren, M., Nordh, L., Belmonte, J. A., Rodrigo, C., Rodriguez Espinosa, J. M., Vidal, L., Mosser, B., Ulla, A., & Gautier, D. 1995 Collision of Shoemaker-Levy 9 fragments A, E, H, L, Q1 with Jupiter: Mid-Infrared light curves. Geophys. Res. Lett. **22,** 1773-1776.

Lieske, J. H. 1977 Theory of motion of Jupiter's Galilean satellites. Astron. Astrophys. **56,** 333-352.

Lieske, J. H. 1994 Galilean satellite ephemerides E4. JPL Engineering Memorandum 314-545, June 19, 1994.

Lindal, G. F., Wood, G. E., Levy, G. S., Anderson, J. D., Sweetnam, D. N., Hotz, H. B., Buckles, B. J., Holmes, D. P., Doms, P. E., Eshleman, V. R., Tyler, G. L., & Croft, T. A. 1981 The atmosphere of Jupiter: An analysis of the Voyager radio occultation measurements. J.G.R. **86,** 8721-8727.

Marsden, B. G. 1993a IAU Circular 5726, March 2, 1993.

Marsden, B. G. 1993b IAU Circulars 5741-5745, April 3, 1993.

Marsden, B. G. 1993c IAU Circular 5800-5801, May 22, 1993.

Marsden, B. G. 1993d IAU Circular 5892, November 22, 1993.

Marsden, B. G. 1993e IAU Circular 5900, December 14, 1993.

Marsden, B. G. 1994a IAU Circulars 5936-5937, February 18-21, 1994.

Marsden, B. G. 1994b Minor Planet Circulars 23106-23107, February 26, 1994.

Martin, T. Z., Orton, G. S., Travis, L. D., Tamppari, L. K., & Claypool, L. 1995 Observation of Shoemaker-Levy impacts by the Galileo Photopolarimeter Radiometer. Science **268,** 1875-1879.

Meadows, V., Crisp, D., Orton, G., Brooke, T., & Spencer, J. 1995 AAT IRIS observations for the SL-9 impacts and initial fireball evolution. In Proceedings of the European SL-9/Jupiter Workshop, (eds. R. West and H. Bohnhardt) pp. 129-134. ESO.

Nakano, S. 1993 IAU Circular 5800, May 22, 1993.

Nicholson, P. D., Gierasch, P. J., Hayward, T. L., McGhee, C. A., Moersch, J. E., Squyres, S. W., Van Cleve, J., Matthews, K., Neugebauer, G., Shupe, D., Weinberger, A., Miles, J. W., & Conrath, B. J. 1995 Palomar observations of the R impact of comet Shoemaker-Levy 9: I. Light curves. Geophys. Res. Lett. **22,** 1613-1616.

Orton, G. S., with help from the NIMS, PPR, SSI and UVS experiment teams 1995a Comparison of Galileo SL-9 impact observations. In Proceedings of the European SL-9/Jupiter Workshop, (eds. R. West and H. Bohnhardt), pp. 75-80. ESO.

Orton, G., A'Hearn, M., Baines, K., Deming, D., Dowling, T., Goguen, J., Griffith, C., Hammel, H., Hoffmann, W., Hunten, D., Jewitt, D., Kostiuk, T. et al. 1995b Collision of comet Shoemaker-Levy 9 with Jupiter observed by the NASA Infrared Telescope Facility. Science **267,** 1277-1282.

Roeser, S. & Bastian, U. 1989 PPM: Positions and proper motions of 181731 stars north of -2.5 degrees declination for equinox and epoch J2000. Astronomisches Rechen-Institut, Heidelberg.

Scotti, J. V., & Melosh, H. J. 1993 Estimate of the size of comet Shoemaker-Levy 9 from a tidal

breakup model. Nature **365**, 733–735.

Sekanina, Z. 1995 The splitting of the nucleus of comet Shoemaker-Levy 9. In Proceedings of the European SL-9/Jupiter Workshop, (eds. R. West and H. Bohnhardt), pp. 43–55. ESO.

Sekanina, Z., & Yeomans, D. K. 1985 Orbital motion, nucleus precession, and splitting of periodic comet Brooks 2. Astron. J. **90**, 2335–2345.

Sekanina, Z., Chodas, P. W., & Yeomans, D. K. 1994 Tidal disruption and the appearance of periodic comet Shoemaker-Levy 9. Astron. Astrophys. **289**, 607–636.

Shoemaker, C. S., Shoemaker, E. M., & Levy, D. 1993 IAU Circular 5725, March 26, 1993.

Standish, E. M. 1990 The observational basis for JPL's DE200, the planetary ephemerides of the Astronomical Almanac. Astron. Astrophys. **233**, 252–271.

Takeuchi, S., Hasegawa, H., Watanabe, J., Yamashita, T., Abe, M., Hirota, Y., Nishihara, E., Okumura, S., & Mori, A. 1995 Near-IR imaging observations of the cometary impact into Jupiter: Time variation of radiation from impacts of fragments C, D, and K. Geophys. Res. Lett. **22**, 1581.

Tancredi, G., Lindgren, M., & Lagerkvist, C.-I. 1993 IAU Circular 5892, November 22, 1993.

Tancredi, G., Lindgren, M., & Rickman, H. 1990 Temporary satellite capture and orbital evolution of comet P/Helin-Roman-Crockett. Astron. Astrophys. **239**, 375–380.

Tozzi, G. P., Richichi, A., & Ferrara, A. 1995 Hi-L temporal resolution near-IR observations of impacts H and Q from Calar Alto and Interpretation. In IAU Colloquium 156: The Collision of Comet P/Shoemaker-Levy 9 and Jupiter, p. 111.

Watanabe, J., Yamashita, T., Hasegawa, H., Takeuchi, S., Abe, M., Hirota, Y., Nishihara, E., Okumura, S., & Mori, A. 1995 Near-IR observation of cometary impacts to Jupiter: Brightness variation of the impact plume of fragment K. Publ. Astron. Soc. Japan **47**, L21.

Yeomans, D. K., & Chodas, P. W. 1993a IAU Circular 5807, May 28, 1993.

Yeomans, D. K., & Chodas, P. W. 1993b Minor Planet Circular 22197, June 4, 1993.

Yeomans, D. K., & Chodas, P. W. 1993c The collision of comet Shoemaker-Levy 9 with Jupiter in July 1994. JPL Interoffice Memorandum 314.10-50, July 21, 1993.

Yeomans, D. K., & Chodas, P. W. 1993d IAU Circular 5909, December 17, 1993.

Yeomans, D. K., & Chodas, P. W. 1994a Comet Shoemaker-Levy 9 impact times. JPL Interoffice Memorandum 314.10-87, August 2, 1994.

Yeomans, D. K., & Chodas, P. W. 1994b Comet Shoemaker-Levy 9 in orbit about Jupiter. Bull. Am. Astron. Soc. **26**, p. 3.

Yeomans, D. K., & Chodas, P. W. 1995 Predictions of close earth approaches of asteroids and comets. In Hazards Due to Comets and Asteroids (ed. T. Gehrels), pp. 241–258. University of Arizona Press.

Zahnle, K., & Mac Low, M.-M. 1995 A simple model for the light curve generated by Shoemaker-Levy 9 impact. J. Geophys. Res. **100**, 16885–